

GENERAL RELATIVISTIC SIMULATIONS OF JET FORMATION IN A RAPIDLY ROTATING BLACK HOLE MAGNETOSPHERE

SHINJI KOIDE

Faculty of Engineering, Toyama University, Gofuku 3190, Toyama 930-8555, Japan

DAVID L. MEIER

Jet Propulsion Laboratory, 4800 Oak Grove Dr. Pasadena, CA 91109, USA.

KAZUNARI SHIBATA

Kwasan and Hida Observatories, Kyoto University, Yamashina, Kyoto, 607-8471, Japan.

TAKAHIRO KUDOH

National Astronomical Observatory, Mitaka, Tokyo 181-8588, Japan

Draft version October 2, 2018

ABSTRACT

To investigate the formation mechanism of relativistic jets in active galactic nuclei and micro-quasars, we have developed a new general relativistic magnetohydrodynamic code in Kerr geometry. Here we report on the first numerical simulation of jet formation in a rapidly-rotating ($a = 0.95$) Kerr black hole magnetosphere. We study cases in which the Keplerian accretion disk is both co-rotating and counter-rotating with respect to the black hole rotation. In the co-rotating disk case, our results are almost the same as those in Schwarzschild black hole cases: a gas pressure-driven jet is formed by a shock in the disk, and a weaker magnetically-driven jet is also generated outside the gas pressure-driven jet. On the other hand, in the counter-rotating disk case, a new powerful magnetically-driven jet is formed inside the gas pressure-driven jet. The newly found magnetically-driven jet in the latter case is accelerated by a strong magnetic field created by frame dragging in the ergosphere. Through this process, the magnetic field extracts the energy of the black hole rotation.

Subject headings: accretion, accretion disks — black hole physics — galaxies: jets — magnetic field — methods: numerical — MHD — relativity

1. INTRODUCTION

Radio jets ejected from radio loud active galactic nuclei (AGNs) sometimes show proper motion with apparent velocity exceeding the speed of light c (Pearson *et al.* 1981, Hughes 1991). The widely-accepted explanation for this phenomenon, called superluminal motion, is relativistic jet flow in a direction along the observer's line-of-sight with a Lorentz factor greater than 2 (Rees 1966). Such relativistic motion is thought to originate from a region very close to the putative supermassive black hole which is thought to power each AGN (Linden-Bell 1969, Rees 1984). On the other hand, the great majority of AGNs are radio quiet and do not produce powerful relativistic radio jets (Rees 1984). These two classes of active objects (radio loud and quiet) are also found in the black hole candidates (BHCs) in our own Galaxy. Objects with superluminal jets, such as GRS 1915+105 and GRO J1655-40, belong to the radio loud class (Mirabel & Rodriguez 1994, Tingay *et al.* 1995). Other objects such as Cyg X-1 and GS 1124-68 are relatively radio quiet and produce little or no jet.

What causes the difference between the two classes? Recent observations of the BHCs in our Galaxy suggest that the Galactic superluminal sources contain very rapidly rotating black holes (normalized angular momentum, $a \equiv J/[GM_{\text{BH}}^2/c] = 0.9 - 0.95$, where G and M_{BH} are the gravitational constant and black hole mass, respectively), while the black holes in Cyg X-1 and GS

1124-68 are spinning much less rapidly ($a = 0.3 - 0.5$) (Cui, Zhang, & Chen 1998). A similar rapidly rotating black hole is also suggested in the AGN of the Seyfert 1 galaxy MCG-6-30-15 by the X-ray satellite ASCA (Iwasawa *et al.* 1996). According to recent (nonrelativistic) studies of magnetically-driven jets from accretion disks by Kudoh & Shibata (1995, 1997a), the terminal velocity of the formed jet is comparable to the rotational velocity of the disk at the foot of the jet. Further nonrelativistic simulations of jet formation confirm these results (Kudo & Shibata 1997b, Ouyed, Pudritz, & Stone 1997), except for the extremely large magnetic field/high jet-power case (Meier *et al.* 1997, Meier 1999) in which very fast jets can be produced. The rotation velocity at the innermost stable orbit of the Schwarzschild black hole ($r = 3r_S$) is $0.5c$, where $r_S = 2GM_{\text{BH}}/c^2$ is the Schwarzschild radius. In addition, it appears that the poloidal magnetic field strength in disks around non-rotating black holes may be not extremely strong if the magnetic field energy density is comparable with that of the radiation (Begelman, Blandford, & Rees 1984, Rees 1984). Therefore, a jet produced by MHD acceleration from an accretion disk around a non-rotating black hole should be sub-relativistic and very weak. In fact, numerical simulations of jet formation in a Schwarzschild metric show only sub-relativistic jet flow (Koide, Shibata, & Kudoh 1999a), except for the case when the initial black hole corona is in hydrostatic equilibrium rather than free fall (Koide, Shibata, & Ku-

doh 1998).

Several mechanisms for relativistic jet formation from rotating black holes have been proposed (Blandford & Znajek 1977, Takahashi *et al.* 1990). However, up until now no one has performed a self-consistent numerical simulation of the dynamic process of jet formation in a rotating black hole magnetosphere. To this end, we have developed a Kerr general relativistic magnetohydrodynamic (KGRMHD) code. In this paper we report briefly on what we believe are some of the first calculations of their kind — simulation of jet formation in a rotating black hole magnetosphere.

2. NUMERICAL METHOD

We use a 3 + 1 formalism of the general relativistic conservation laws of particle number, momentum, and energy and Maxwell equations with infinite electric conductivity (Thorne, Price, & Macdonald 1986). The Kerr metric, which describes the spacetime around a rotating black hole, is used in the calculation. When we use Boyer-Lindquist coordinates, $x^0 = ct$, $x^1 = r$, $x^2 = \theta$, and $x^3 = \phi$, the Kerr metric $g_{\mu\nu}$ is written as follows,

$$ds^2 = g_{\mu\nu} dx^\mu dx^\nu = -h_0^2 (cdt)^2 + \sum_{i=1}^3 h_i^2 (dx^i)^2 - 2h_3 \Omega_3 c dt dx^3. \quad (1)$$

By modifying the lapse function in our Schwarzschild black hole code ($\alpha = \sqrt{1 - r_S/r}$) to be $\alpha = \sqrt{h_0^2 + \Omega_3^2}$, and adding some terms of Ω_3 to the time evolution equations, we were able to develop a KGRMHD code relatively easily. (See Appendix C in Koide, Shibata, & Kudoh 1999a for more details on this procedure and the meaning of symbols used.)

We use the Zero Angular Momentum Observer (ZAMO) system for the 3-vector quantities, such as velocity \mathbf{v} , magnetic field \mathbf{B} , and so on. For scalars, we use the frame comoving with the fluid flow. The simulation is performed in the region $0.75r_S \leq r \leq 20r_S$, $0 \leq \theta \leq \pi/2$ with 210×70 mesh points, assuming axisymmetry with respect to the z -axis and mirror symmetry with respect to the plane $z = 0$. A free boundary condition is employed at $r = 0.75r_S$ and $r = 20r_S$. In the simulations, we use simplified tortoise coordinates, $x = \log(r/r_H - 1)$, where r_H is the radius of the black hole horizon. To avoid numerical oscillations, we use a simplified TVD method (Davis 1984, Koide, Nishikawa & Mutel 1996, Koide 1997, Koide, Shibata, & Kudoh 1999a). We checked the KGRMHD code by computing Kepler motion around a rotating black hole and comparing with analytic results (Shapiro & Teukolsky 1983).

3. RESULTS

The simulations were performed for two cases in which the disk co-rotates and counter-rotates with respect to the black hole rotation. Figures 1a-c illustrate the time evolution of the counter-rotating disk case and Fig. 1d the final state of the co-rotating case. These figures show the rest mass density (color), velocity (vectors), and magnetic field (solid lines) in $0 \leq R \equiv r \sin \theta \leq 7r_S$, $0 \leq z \equiv r \cos \theta \leq 7r_S$. The black region at the origin shows the inside of the black hole horizon. The angular

momentum parameter of the black hole is $a = 0.95$ and the radius is $r_H = 0.656r_S$. The initial state in the simulation consists of a hot corona and a cold accretion disk around the black hole (Fig. 1a). In the corona, plasma is assumed to be in nearly stationary infall, with the specific enthalpy $h/\rho c^2 = 1 + \Gamma p/[(\Gamma - 1)\rho c^2] = 1.3$, where ρ is the rest mass density, p is the pressure, and Γ is specific heat ratio and set $\Gamma = 5/3$. Far from the hole, it becomes the stationary transonic solution exactly. The accretion disk is located at $|\cot \theta| \leq 0.125$, $r \geq r_D = 3r_S$ and the initial velocity of the disk is assumed to be the velocity of a circular orbit around the Kerr black hole. The co-rotating disk is stable, but the counter-rotating disk is unstable in the region $R \leq 4.4r_S$. Except for the disk rotation direction, we use the same initial conditions in both cases. The mass density of the disk is 100 times that of the corona at the inner edge of the disk. The mass density profile is given by that of a hydrostatic equilibrium corona with a scale height of $r_c \sim 3r_S$. The disk is in pressure balance with the corona, and the magnetic field lines are perpendicular to the accretion disk. We use the azimuthal component of the vector potential A_ϕ of the Wald solution to set the magnetic field, which provides a uniform magnetic field far from the Kerr black hole (Wald 1974). Here the magnetic field strength far from the black hole is $0.3\sqrt{\rho_0 c^2}$, where ρ_0 is the initial corona density at $r = 3r_S$. However, we do not use the time component of the vector potential A_t from Wald solution; instead, we use the ideal MHD condition $\mathbf{E} + \mathbf{v} \times \mathbf{B} = \mathbf{0}$ to determine the electric field \mathbf{E} . Here the Alfvén velocity and plasma beta value at the disk ($r = 3.5r_S$) are $v_A = 0.03c$ and $\beta \sim 3.4$, respectively.

Figure 1b shows the state at $t = 30\tau_S$, where τ_S is defined as $\tau_S \equiv r_S/c$. By this time the inner edge of the disk has rotated 0.75 cycles, *if* we assume the edge is at $R = 3r_S$.¹ Actually, the edge falls toward the black hole and rotates faster at $R = 2r_S$. The rapid infall produces a shock at $R = 3.1r_S$, and the high pressure behind it begins to produce the jet. This is the same pressure-driven jet formation process seen previously in the Schwarzschild case (Koide, Shibata, & Kudoh 1999a).

Figure 1c shows the final state of the counter-rotating disk case at $t = 47\tau_S$ when the inner edge of the disk rotated 1.2 cycles. The accretion disk continues to fall rapidly toward the black hole, with the disk plasma entering the ergosphere and then crossing the horizon, as shown by the crowded magnetic field lines near $r = 0.75r_S$. The magnetic field lines become radial due to dragging by the disk infall near the black hole. The jet is ejected almost along the magnetic field lines. Its maximum total and poloidal velocities are the same, $v = v_p = 0.44c$ at $R = 3.2r_S$, $z = 1.6r_S$. The mass density plot (color) shows that the jet consists of two layers. One is an inner, low density, fast, magnetically-driven jet and the other is an outer, high density, slow, gas pressure-driven jet. The latter comes from the disk near the shock at $R = 3.1r_S$ and is, therefore, similar to the gas pressure-driven jet of Koide, Shibata, & Kudoh (1998). The former is new and has never been seen in the Schwarzschild black hole case. It comes from the disk near the ergosphere, and is accelerated as follows. As there is no stable orbit at $R \leq 4.4r_S$,

¹To calculate inner disk rotation cycles, in this paper we always will assume that the inner edge is located at $R = 3r_S$, regardless of how far inward the edge actually has accreted.

the disk falls rapidly into the ergosphere. Inside the static limit, the velocity of frame dragging exceeds the speed of light ($c\Omega_3/\alpha > c$), causing the disk to rotate in the *same* direction of the black hole rotation (relative to the fixed Boyer-Lindquist frame), even though it was initially counter-rotating. The rapid, differential frame dragging greatly enhances the azimuthal magnetic field, which then accelerates the flow upward and pinches it into a powerful collimated jet.

Figure 1d shows a snapshot of the co-rotating disk case at $t = 47\tau_S$. The disk stops its infall near $R = 3r_S$ due to the centrifugal barrier with a shock at $r = 3.4r_S$. The high pressure behind the shock causes a gas pressure-driven jet with total and poloidal velocities of $v = v_p = 0.30c$ at $R = 3.4r_S$, $z = 2.4r_S$. A detailed analysis shows that a weak magnetically-driven jet is formed outside the gas pressure-driven jet with maximum total and poloidal velocities of $v = 0.42c$ and $v_p = 0.13c$, respectively. This two-layered shell structure is similar to that of Schwarzschild black hole case (Koide, Shibata, & Kudoh 1998). The centrifugal barrier makes the disk take much long time to reach the ergosphere, which causes the difference between the co-rotating and counter-rotating disk cases.

To more fully illustrate the physics of the jet formation mechanism, in figure 2 we show the plasma beta, $\beta \equiv p/(B^2/2)$ (color) and the toroidal component of the magnetic field, B_ϕ (contour) in the counter-rotating and co-rotating disk cases at $t = 47\tau_S$. The blue color shows the region where magnetic field dominates the gas pressure; light red—yellow shows where gas pressure is dominant; and solid contour line shows negative azimuthal magnetic field ($B_\phi < 0$), while the broken line the positive value ($B_\phi > 0$). The toroidal component of the magnetic field B_ϕ is negative and its absolute value is very large above the black hole in both cases. The field increases to more than 10 times the initial magnetic field. This amplification is caused by the shear of the plasma flow in the Boyer-Lindquist frame due to the frame dragging effect of the rotating black hole (Yokosawa, Ishizuka, & Yabuki 1991, Yokosawa 1993, Meier 1999). Under the simplifying assumption that the plasma is at rest in the ZAMO frame, the general relativistic Faraday law of induction and ideal MHD condition yield,

$$\frac{\partial B_\phi}{\partial t} = f_1 B_r + f_2 B_\theta, \quad (2)$$

where $f_1 = c(h_3/h_1)\partial(\Omega_3/h_3)/\partial r$, and $f_2 = c(h_3/h_2)\partial(\Omega_3/h_3)/\partial\theta$. This expression is almost identical to that of ω -dynamo effect from the field of the terrestrial magnetism. Noted that f_2 is one order smaller than f_1 when $a \sim 1$.

Where does the magnetic field amplification energy comes from? It does not come from the gravitational energy or thermal energy of the disk, because frame dragging effect occurs even when the plasmas of the disk and corona are rest and cool. The only other possible energy source is the rotation of the black hole itself. Indeed, the increase in the azimuthal magnetic field component (eq. (2)) depends on the shear of the rotational variable Ω_3 . We conclude that the amplification energy of the magnetic field is supplied by extraction of the rotational energy of the black hole.

The distribution of the plasma beta (β) and the azimuthal component of the magnetic field (B_ϕ) of the counter-rotating and co-rotating disk cases are quite different. In the co-rotating disk case, they are similar to those of the Schwarzschild black hole case. In the counter-rotating disk case, the outer part has a positive azimuthal component of the magnetic field ($B_\phi > 0$), which is caused by the counter-rotating disk, and the outer part has the high plasma beta. The inner part has a negative azimuthal magnetic field ($B_\phi < 0$) and low plasma beta. Note that the very high plasma beta region (yellow region) is outside of the jet; at this point it has almost stopped and eventually will fall into the black hole. The negative azimuthal magnetic field is caused by the disk around the ergosphere, where the disk rotates in the same direction as the black hole in the Boyer-Lindquist frame.

To confirm the jet acceleration mechanism, we estimate the power from the electromagnetic field, $W_{EM} = \mathbf{v} \cdot (\mathbf{E} + \mathbf{J} \times \mathbf{B})$ and the gas pressure, $W_{gp} = -\mathbf{v} \cdot \nabla p$ along the line, $z = 1.1r_S$ which crosses the jet foot (Fig. 3). At $t = 47\tau_S$, the gas pressure is dominant in the co-rotating disk case (Fig. 3b). However, in the counter-rotating disk case, the electromagnetic power is dominant near the black hole even through the gas pressure power is the same as that of the co-rotating disk case (Fig. 3a). The magnetically-driven jet in this latter case is accelerated by the magnetic field anchored to the ergospheric disk. The frame dragging effect rapidly rotates the disk in the same direction as the black hole rotation, increasing the azimuthal component of the magnetic field and the magnetic tension which, in turn, accelerates the plasma by the magnetic pressure and centrifugal force, respectively. (A detailed analysis shows that both component of the magnetic forces are comparable.) This mechanism of jet production, therefore, is a kind of Penrose process that uses the magnetic field to extract rotational energy of the black hole and eject a collimated outflow from very near the horizon.

4. DISCUSSION

We have presented general relativistic simulations of jet formation from both counter-rotating and co-rotating disks in a Kerr black hole magnetosphere. We have found that jets are formed in both cases. At the time when the simulations were stopped ($t = 47\tau_S$ ($53\tau_S$), after the inner edge of the disk had rotated 1.2 (1.4) cycles in the counter-rotating (co-rotating) disk case) the poloidal velocities of the jets were $v \sim 0.4c$ (counter-rotating), $\sim 0.3c$ (co-rotating), both sub-relativistic. In the co-rotating disk case, the jet has a two-layered structure: inner, gas pressure-driven jet and outer, magnetically-driven jet. On the other hand, in the counter-rotating case, a new magnetically-driven jet has been found inside the gas pressure-driven jet. The new jet is accelerated by the magnetic field induced by the frame dragging effect in the ergosphere. In this case, existence of a magnetically-driven jet is not clear outside the gas pressure-driven jet. A longer term simulation may show a three-layered structure including the outer, magnetically-driven jet.

Unfortunately, the counter-rotating (co-rotating) disk case could not be continued beyond $t = 47\tau_S$ ($t = 53\tau_S$) because of numerical problems. We have performed one other case previously — the infall of a magnetized non-

rotating disk into a rapidly-rotating black hole (Koide, Meier, Shibata, & Kudoh 1999b). The disk falls toward the black hole more rapidly than the counter-rotating case. At later times (after almost two inner disk turns) it developed a *relativistic* jet with a velocity of $v \sim 0.9c$ (Lorentz factor ~ 2). We believe that, if we had been able to perform longer-term simulations here, in at least the counter-rotating disk case the magnetically-driven jet also would have been accelerated to relativistic velocities (and possibly the co-rotating case as well). Despite its low speed, the magnetically-driven jet in the counter-rotating disk case is nevertheless noteworthy because it extracts rotational energy from the black hole. While the process is similar to the Blandford-Znajek mechanism (Blandford & Znajek 1977), it appears more closely related to the model of Takahashi *et al.* (1990). In our case, the electromagnetic field energy is transformed immediately into kinetic energy in the jet. A more detailed analysis and further calculations will be reported in our next paper.

Recently, Wardle *et al.* (1998) detected circularly polarized radio emission from the jets of the archetypal quasar 3C279. They concluded that electron-positron pairs are

important components of the jet plasma. Similar detections in three other radio sources have been made (Homan *et al.* 1999), which suggests that, in general, extragalactic radio jets may be composed mainly of an electron-positron pair plasma. The electron-positron plasma is probably produced very near the black hole. The mechanism we have investigated here, magnetically-driven jet powered by extraction of rotational energy of a black hole, is a strong candidate for explaining the acceleration of such electron-positron jets.

S. K. thanks M. Inada-Koide for discussions and important comments for this study. We thank K.-I. Nishikawa, M. Takahashi, A. Tomimatsu, P. Hardee, and J.-I. Sakai for discussions and encouragement. We appreciate the support of the National Institute for Fusion Science and the National Astronomical Observatory in the use of their super-computers. Part of this research was carried out at the Jet Propulsion Laboratory, California Institute of Technology, under contract with the National Aeronautics and Space Administrations.

REFERENCES

- Begelman, M.C., Blandford, R.D., Rees, M.J. 1984, Review of Modern Physics, **56**, 255.
- Belloni, T., van der Klis, M., Lewin, W. H. G., van Paradijs, J., Dotani, T., Mitsuda, K., & Miyamoto, S. 1997, A & A **322**, 857.
- Blandford, R. D. & Payne, D. G. 1982, MNRAS **199**, 883.
- Blandford, R. D. & Znajek, R. 1977, MNRAS **179**, 433.
- Cui, W., Zhang, S. N., & Chen, W. 1998, ApJ **484**, 383.
- Cui, W., Zhang, S. N., Focke, W., & Swank, J. H. 1997, MNRAS **290**, L65.
- Davis, S. F. 1984, NASA Contractor Rep. 172373, ICASE Rep. No. 84-20.
- Homan, D. C., Wardle, J. F. C., Roberts, D. H., and Ojha, R. 1999, preprint.
- Hughes, P. A. 1991, eds., *Beams and Jets in Astrophysics* (Cambridge University Press, New York).
- Iwasawa, K., Fabian, A. C., Reynolds, C. S., Nandra, K., Otani, C., Inoue, H., Hayashida, K., Brandt, W. N., Dotani, T., Kunieda, H., Matsuoka, M., Tanaka, Y. 1996, MNRAS, **282**, 1038.
- Koide, S. 1997, ApJ **478**, 66.
- Koide, S., Nishikawa, K.-I., & Mutel, R. L. 1996, ApJ **463**, L71.
- Koide, S., Shibata, K., & Kudoh, T. 1998, ApJ **495**, L63.
- Koide, S., Shibata, K., & Kudoh, T., 1999a, ApJ **522**, 175.
- Koide, S., Meier, D. L., Shibata, K., & Kudoh, T. 1999b, in Proc. 19th Texas Symp. on Relativistic Astrophysics, ed. E. Aubourg, T. Montmerle, & J. Paul (World Scientific Press, Paris) in press.
- Kudoh, T. & Shibata, K. 1995, ApJ **452**, L41.
- Kudoh, T. & Shibata, K. 1997a, ApJ **474**, 362.
- Kudoh, T. & Shibata, K. 1997b, ApJ **476**, 632.
- Linden-Bell, D. 1969, Nature **223**, 690.
- Meier, D. L. 1999, ApJ **522**, in press.
- Meier, D. L., Edgington, S., Godon, P., Payne, D. G., & Lind, K. R. 1997, Nature **388**, 350.
- Mirabel, I. F. & Rodriguez, L. F. 1994, Nature **371**, 46.
- Morgan, E. H., Remillard, R. A., & Greiner, J. 1977, ApJ **482**, 993.
- Ouyed, R., Pudritz, R. E., & Stone, J. M. 1997, Nature **385**, 409.
- Pearson, J. J. 1981, *et al.* Nature **290**, 365.
- Rees, M. J. 1966, Nature **211**, 468.
- Rees, M. J. 1984, Ann. Rev. Astron. Ap. **22**, 471.
- Remillard, R. A., Morgan, E. H., McClintock, J. E., Bailyn, C. D., Oroszek, A., & Greiner, J. 1999, in Proc. 18th Texas Symp. on Relativistic Astrophysics, ed. A. Olinto, J. Frieman, & D. Schramm (World Scientific Press, Singapore) in press.
- Shapiro, S. L. & Teukolsky, S. A. 1983, *Black Holes, White Dwarfs, and Neutron Stars*, (John Wiley & Sons Inc., New York)
- Shibata, K. & Uchida, Y. 1986, PASJ **38**, 631.
- Takahashi, M., Nitta, S., Tatematsu, Y., & Tomimatsu, A. 1990, ApJ **363**, 206.
- Thorne, K. S., Price, R. H., & Macdonald, D. A. 1986, *Membrane Paradigm* (Yale University Press, New Haven and London).
- Tingay, S. J. 1995, *et al.* Nature **374**, 141.
- Uchida, Y. & Shibata, K. 1985, PASJ **37**, 515.
- Wald, R. M. 1974, Phys. Rev. D **10**, 1680.
- Wardle, J. F. C., Homan, D. C., Ojha, R., & Roberts, D. H. 1998, Nature **395**, 457.
- Yokosawa, M. 1993, PASJ **45**, 207.
- Yokosawa, M., Ishizuka, T., & Yabuki, Y. 1991, PASJ **43**, 427.

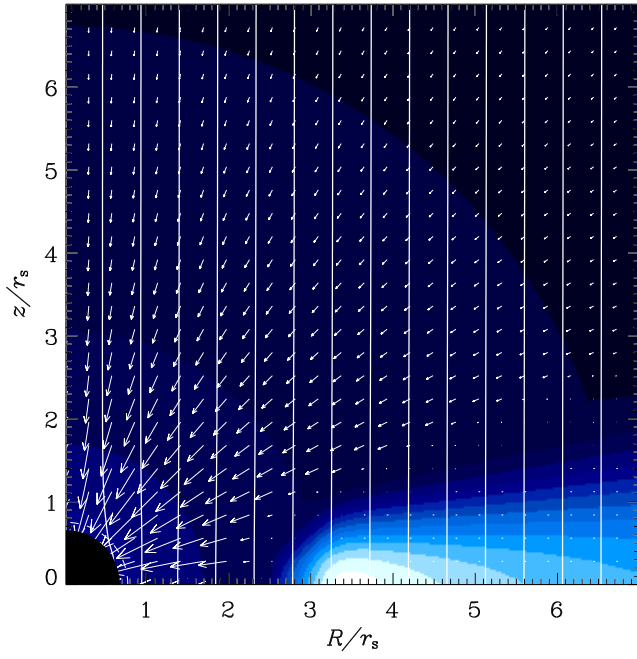
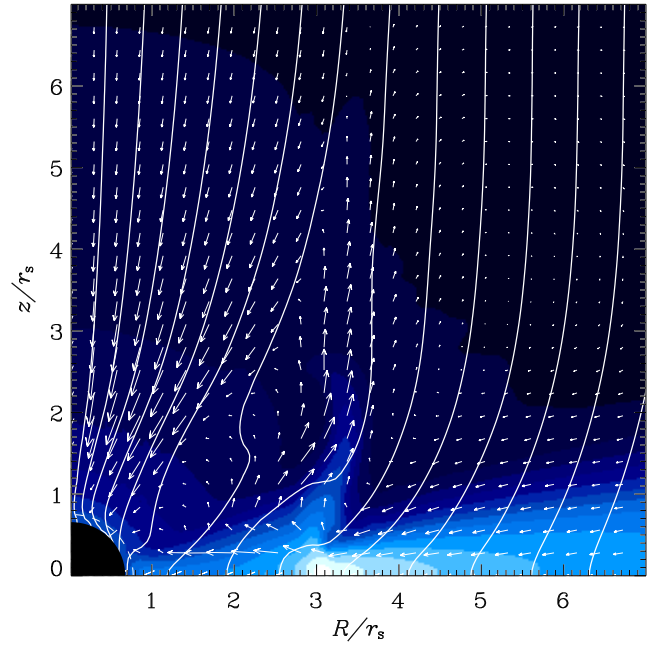
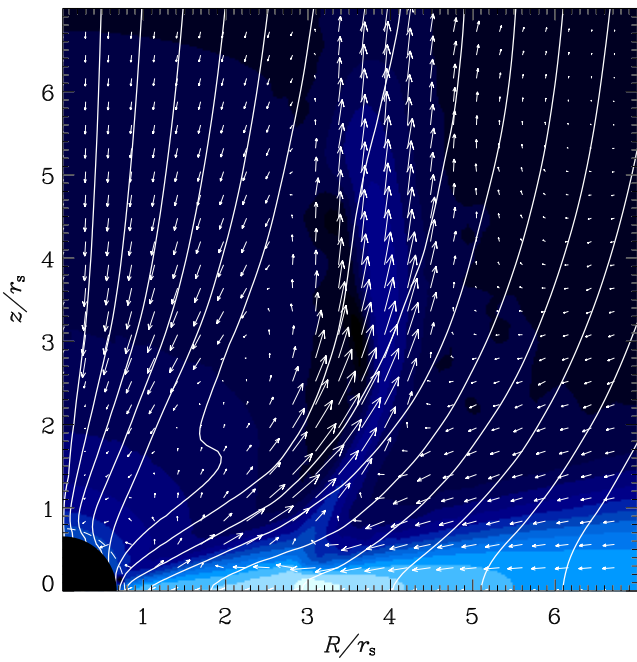
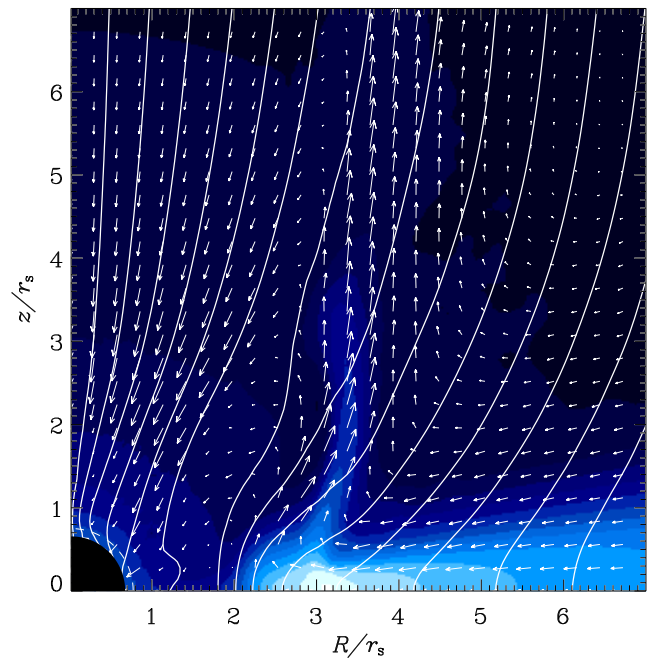
Figure Captions

Fig. 1. Time evolution of jet formation in the counter-rotating disk case and the final state of the co-rotating disk case. Color shows the logarithm of the proper mass density; vectors indicate velocity; solid lines show the poloidal magnetic field. The black fan-shaped region at the origin shows the horizon of the Kerr black hole ($a = 0.95$). The dashed line near the horizon is the inner boundary of the calculation region.

At $t = 0$ and $t = 30\tau_S$ the state of the co-rotating and counter-rotating disk cases are almost identical. However, at $t = 47\tau_S$, while the infall of the disk in the co-rotating disk stops (due to a centrifugal barrier), the unstable orbits of the counter-rotating disk plasma continue to spiral rapidly toward the black hole horizon. This difference causes the magnetohydrodynamic jet formation mechanisms in the two cases to differ drastically, resulting in a powerful jet emanating from deep within the ergosphere.

Fig. 2. Plasma beta (color) and azimuthal component of the magnetic field B_ϕ (contour) in the counter-rotating and co-rotating disk cases. Solid lines show negative value of B_ϕ and the dashed lines positive values. The two cases differ significantly in structure, with the jet in the counter-rotating case originating much closer to the black hole.

Fig. 3. Power contribution to jet acceleration along the line, $z = 1.1r_S$ due to the gas pressure (W_{gp}) and the electromagnetic force (W_{EM}) for both the counter-rotating and co-rotating disk cases. The jet in the counter-rotating disk case is accelerated mainly by electromagnetic forces, while that in the co-rotating disk is accelerated mainly by gas pressure. Note that, while the power in the gas jet component is comparable in the two cases, the power in the MHD jet component is nearly two orders of magnitude greater in the counter-rotating case than the co-rotating case.

(a) counter-rotating disk
t=0(b) counter-rotating disk
t=30(c) counter-rotating disk
t=47(d) co-rotating disk
t=47

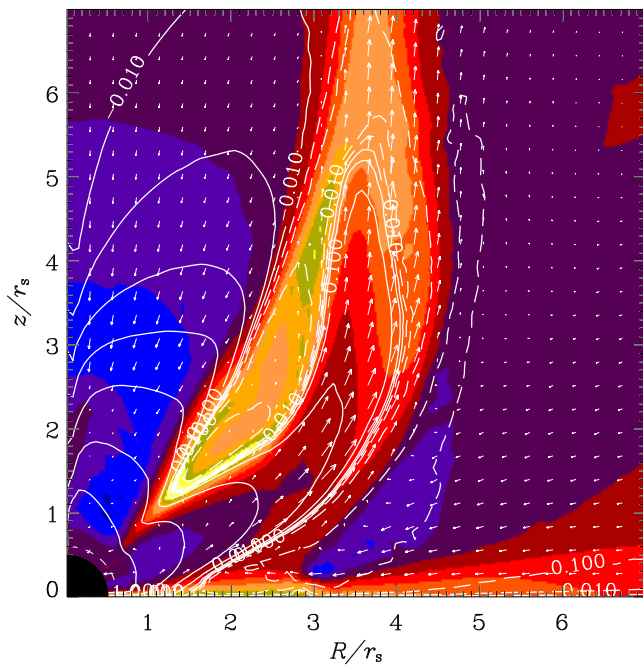
→
c



Fig. 1.—

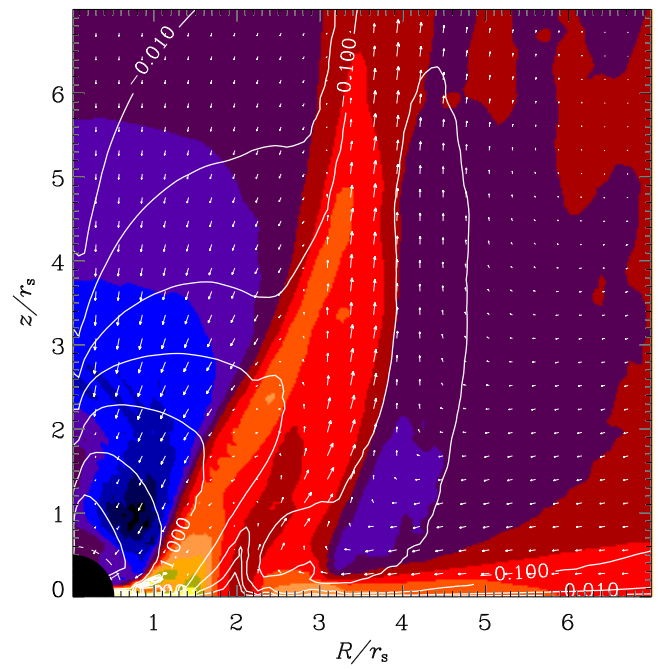
(a) counter-rotating disk

$t=47$



(b) co-rotating disk

$t=47$



\rightarrow
 c

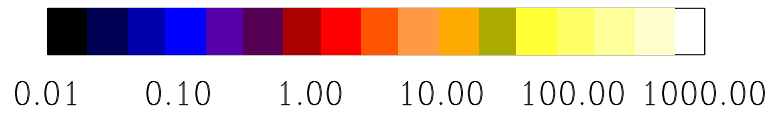
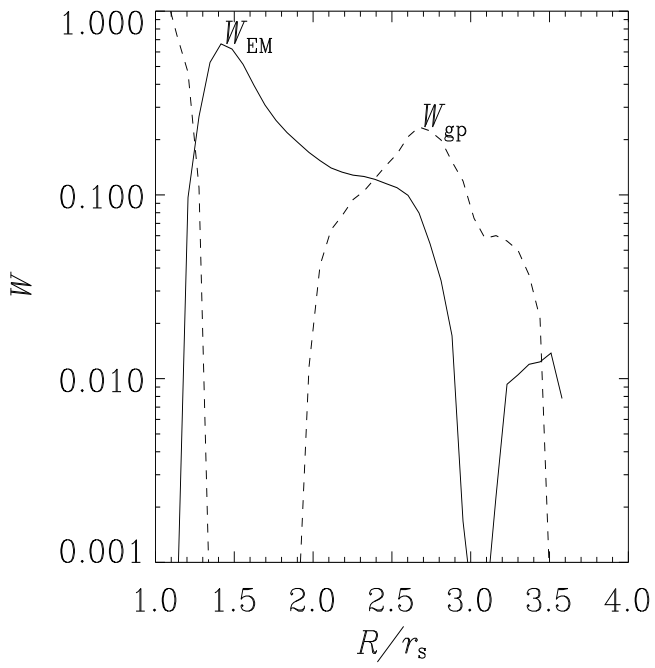


Fig. 2.—

(a) counter-rotating disk
 $t=47, z=1.1$



(b) co-rotating disk
 $t=47, z=1.1$

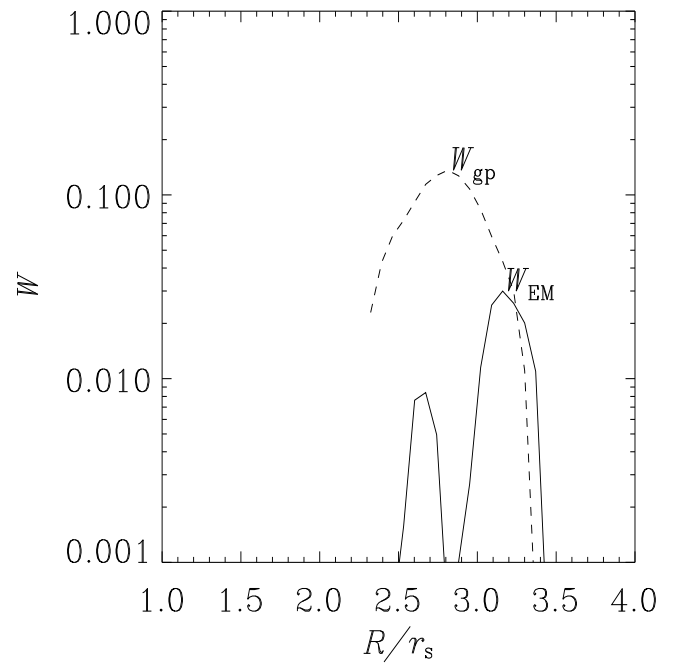


Fig. 3.—